

Effect of geotextile cover on snow and ice melt on Triangular Glacier, the north-eastern Antarctic Peninsula

Zbyněk Engel^{1*}, Kamil Láska², Michael Matějka² and Ondřej Neděľčev¹

¹Charles University, Faculty of Science, Department of Physical Geography and Geoecology, Albertov 6, 128 00 Praha, Czech Republic

²Masaryk University, Faculty of Science, Department of Geography, Kotlářská 2, 611 37 Brno, Czech Republic

Abstract

A prominent increase in air temperature during the last decade has prompted summer melting and surface lowering of glaciers in the Antarctic Peninsula region. Accelerated mass loss from small land-terminating glaciers on James Ross Island has attracted research attention to local conditions of snow and ice melt that remain poorly known. This study focuses on the potential effects of non-woven geotextile on snow and ice melt on the surface of Triangular Glacier. The measurements of surface elevation changes reveal a total melt-season ablation of 1.3 to 1.6 m during the summer 2021/22. Over half of the melt season the surface lowering ranged from 0.5 m at the shaded glacier head to 0.8 m on the glacier surface unconstrained by topography, implying the importance of local topography on surface melting. The protection of glacier surface with non-woven geotextile covers reduced the snow and ice ablation by 40 to 69%. The lower effect of this protection is attributed to less intense surface melt at the shaded site. The efficiency of the geotextile cover is consistent with the reported values from mid-latitude sites but it is higher compared to the recently reported estimates from a high-elevation region in Asia.

Key words: snow, glacier, surface melt, geotextile, Antarctic Peninsula

DOI: 10.5817/CPR2022-2-19

Introduction

Snow and ice at the glacier surface ablate more slowly in Antarctica than in lower-latitude regions. Melt and sublimation, the primary mechanisms of surface ablation, are driven by the annual net flux of energy from the overlying atmosphere that decreases by 150 W m^{-2} between 20° and 80°S latitude (Peixoto and

Received October 23, 2022, accepted January 3, 2023.

*Corresponding author: Z. Engel <zbynek.engel@natur.cuni.cz>

Acknowledgements: We thank Filip Haiduk, Chris Stringer, and the crew of Johann Gregor Mendel station for the fieldwork support, reviewers for helpful comments and reviews of this manuscript. We are also grateful to Czech Antarctic Research Programme of Masaryk University and Environmental Measuring Systems Brno (Czech Republic) for the long-term support of research-grade devices and meteorological systems. The Pléiades DEM used in this study was provided by the Pléiades Glacier Observatory initiative of the French Space Agency (Centre National d'Études Spatiales, CNES).

Funding: The research was funded by the Czech Science Foundation (project GC20-20240S) and the project of Masaryk University (MUNI/A/1393/2021).

Oort 1992). Sublimation prevails in very cold environments where subfreezing temperatures preclude melting. In the extreme conditions of Dry Valleys, sublimation may account for loss rates of up to 0.4 m yr^{-1} (Bliss *et al.* 2011). Surface melt tends to dominate the loss of ice masses on the sub-Antarctic islands where melt rates may exceed 2 m yr^{-1} (Thost and Truffer 2008, Navarro *et al.* 2013). Melt continues to increase with solar radiation and summer temperatures towards lower latitudes lowering glacier surface in excess of $>10 \text{ m yr}^{-1}$ (Cuffey and Paterson 2010). Moreover, recent atmospheric warming in the Antarctic Peninsula region coupled with orographically-induced downslope flow over the Peninsula has increased surface melting on ice shelves and land-terminating glacier on the eastern side of the Peninsula (Engel *et al.* 2022, Laffin *et al.* 2022).

The rapid mass loss from glaciers has serious environmental consequences for the global sea-level and climate system (Hock *et al.* 2017). The ice loss also affects river systems, which represent the essential habitat for a variety of species and the resource of water for hydroelectric production, irrigation, and municipal water supplies (Burkhart *et al.* 2017). Finally, glaciers have aesthetic, cultural, and recreational value for local inhabitants and tourists (Orlove *et al.* 2008). The rapidly increasing mass loss of glaciers reported since the late-20th century from high-altitude and polar regions (*e.g.* Hugonnet *et al.* 2021) attracted attention to global glacier projections (Edwards *et al.* 2021, and references therein) and strategies aimed at the reduction of snow and ice melt (Skogsborg and Lundberg 2005, Olefs and Obleit-

ner 2007, Oerlemans *et al.* 2017). During subsequent years, several techniques were developed to increase mass accumulation or reduce snow and ice melt (Huss *et al.* 2021).

Covering glaciers with the geotextile during the melt season appeared to be the most effective method that decreased the surface melt up to 70% (Olefs and Fischer 2008, Huss *et al.* 2021). The effect of this method results mainly from high albedo and low thermal conductivity of the geotextile, which reflects a large amount of the direct incoming solar radiation and reduces turbulent heat fluxes (Olefs and Lehning 2010). After the refinement of the geotextile covering strategy on glaciers in the European Alps (Huss *et al.* 2021 and references therein), it was applied on snowfields in the Lesser Caucasus (Nestler *et al.* 2014) and glaciers in the Eastern Tien Shan (Liu *et al.* 2022) and Qionglai Shan (Xie *et al.* 2022). All these mountain ranges are located in mid-latitudes where high summer intensity of net radiation and strong sensible heat flux generate intense melting at the glacier surface (Sauter and Galos 2016). In the polar regions, lower solar elevation reduces the daily maximum intensity of downward solar radiation whereas colder air and reduced vapour pressure of water enlarge sublimation and the amount of latent heat fluxes (Cuffey and Paterson 2010). The differences in the energy budget for mid- and high-latitude glaciers imply that the geotextile cover should be less effective in the melt reduction in the polar region. Here we examine this hypothesis testing the effect of the non-woven geotextile on snow and ice melt on the surface of Triangular Glacier.

Material and Methods

Triangular Glacier (GLIMS ID: G302151 E63856S; $63^{\circ}51'01''$ to $63^{\circ}51'35''\text{S}$, $57^{\circ}50'26''$ to $57^{\circ}51'25''\text{W}$) is located in the north-western part of James Ross Island,

which is situated around 80 km from the northern tip of the Antarctic Peninsula (Fig. 1a). Headwall cliffs 120 to 200 m high bound the upper part of this cirque

glacier that descends towards the braid-plain of Abernethy Flats (Fig. 1b). Prominent scree slopes form at the base of the cliffs on the glacier head but supraglacial debris is limited on the lower parts of the glacier. The glacier extends over the elevation range of 329–104 m a.s.l. and covers the area of $0.524 \pm 0.004 \text{ km}^2$. The glacier with the maximum measured ice thickness of $103 \pm 5 \text{ m}$ is inclined to the south-west and its surface has a mean

slope of 15° . Annual mass balance values have been negative since the mass-balance year 2015/16 yielding a net mass loss of $-1.66 \pm 0.83 \text{ m}$ in water equivalent over the period 2015–2020 (Engel et al. 2022). The largest mass loss since the beginning of mass-balance measurements was observed during the 2019/20 melt season when a prominent heatwave affected the Antarctic Peninsula region (González-Herrero et al. 2022).

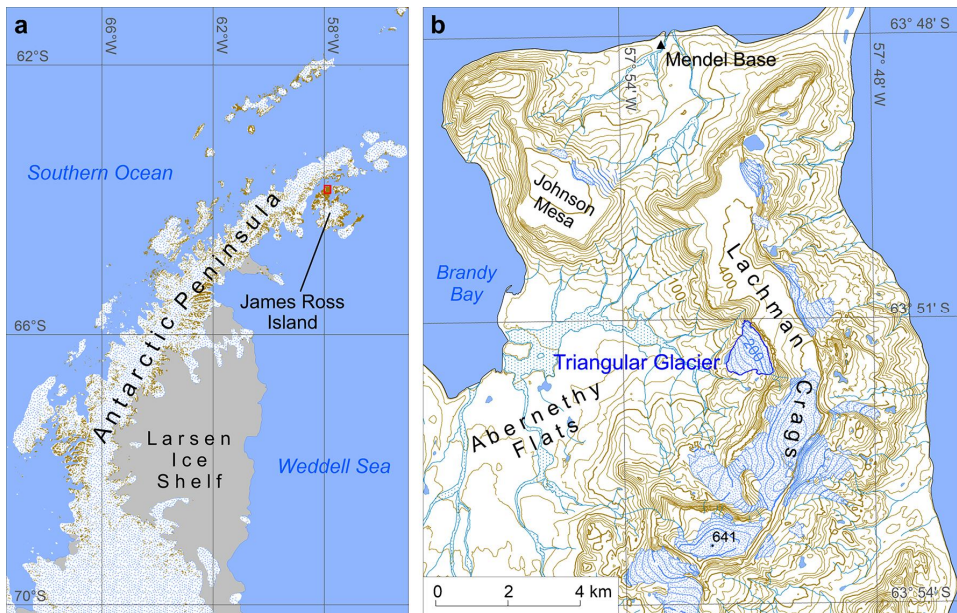


Fig. 1. (a) Location of the study area (red rectangle) in the north-eastern part of the Antarctic Peninsula. (b) Topography of the study area with the location of Triangular Glacier after Czech Geological Survey (2009)^[1].

Local climate conditions on the Triangular Glacier during the summer 2021/22 were recorded using an automatic weather station (AWS) installed in the middle part of the glacier (Fig. 2). Near-surface air temperature was measured using the EMS33H probe (EMS Brno, Czech Republic) with a built-in semiconductor type sensor installed at 2 m above the glacier surface in a radiation shield. The temperature data were measured and recorded every 30 min-

utes. Daily and monthly mean air temperatures were calculated based on the 30-minutes instantaneous data. The positive degree day (PDD) approach was used to calculate snow/ice surface melt, using the number of PDD computed as an integral of positive air temperature (in $^\circ\text{C}$) over a time interval (Hock 2003). A surface elevation change of snow and ice around AWS was monitored using a sonic distance sensor (Judd Communication,

USA) with the accuracy of ± 0.01 m. The instantaneous distance data were acquired in 4-hour intervals during the period from 1 December 2021 to 23 February 2022. In the next step, the raw sonic signal was corrected for the actual air temperature and set at a fixed surface elevation of 200 cm

on 1 December 2021. Instantaneous sonic data were also used to estimate the total sum of positive (snow accumulation) and negative (snow melting, wind drift, or sublimation) surface elevation changes that occurred at the AWS site each month.

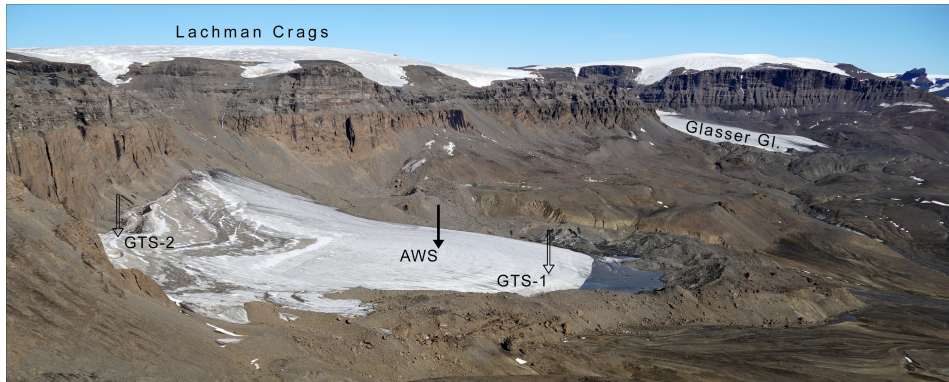


Fig. 2. Triangular Glacier with the location of automatic weather station (AWS) and geotextile test sites (GTS). View from the north.

In addition to the AWS, the surface elevation of snow and ice was measured at 11 ablation stakes distributed across the glacier surface, at experimental sites on the terminus (GTS-1 site) and the top of the glacier (GTS-2) at the foot of the cirque headwall (Figs. 2 and 3). The surface elevation at the lower site was recorded from 6 January to 23 February 2022 using a time-lapse camera (BUNATY, Czech Republic) and ablation stakes drilled into the glacier. At the glacier head, the height of ablation stakes above the surface was measured on 6 and 20 January and 23 February using a tape measure. The elevation changes at the experimental sites were determined for the natural glacier surface and for the sites covered with the non-woven geotextile geoNETEX S 300 made of polypropylene (JUTA, Czech Republic). In order to evaluate the effect of protective covering, the geotextile with the fabric mass of 300 g m^{-2} and thickness of 3.2 mm (at 2 kPa) was placed on the experimental

sites with the area of 4 m^2 , and fixed to the glacier.

Snow density was measured in pits at the experimental sites and AWS between 17 and 29 January 2022. The measured values yield a mean density of 388 kg m^{-3} that was used to convert height differences of the snowpack to metres in water equivalent (m w.e.). The lowering of bare glacier surface was converted assuming an ice density of 900 kg m^{-3} . The coordinates and the elevation of the ablation stakes, the AWS, and the experimental sites were recorded with a Trimble Geo7X receiver (Trimble, USA), and differentially corrected using the data collected at the Mendel Base reference station ($63^{\circ}48'S$ and $57^{\circ}53'W$). The aspect and slope of the Triangular Glacier at the experimental sites were derived from the 2020 Pléiades DEM of the French Space Agency (CNES), a topographic shielding factor and the sunshine duration for these sites over the summer season (DJF) were determined using

the Shielding tool (Li 2013) and ArcGIS (Esri, USA) Solar Radiation tool, respectively. Clear-sky downward shortwave ra-

diation flux at noon over the study sites is based on the Bird and Hulstrom's model (Bird and Hulstrom 1981).

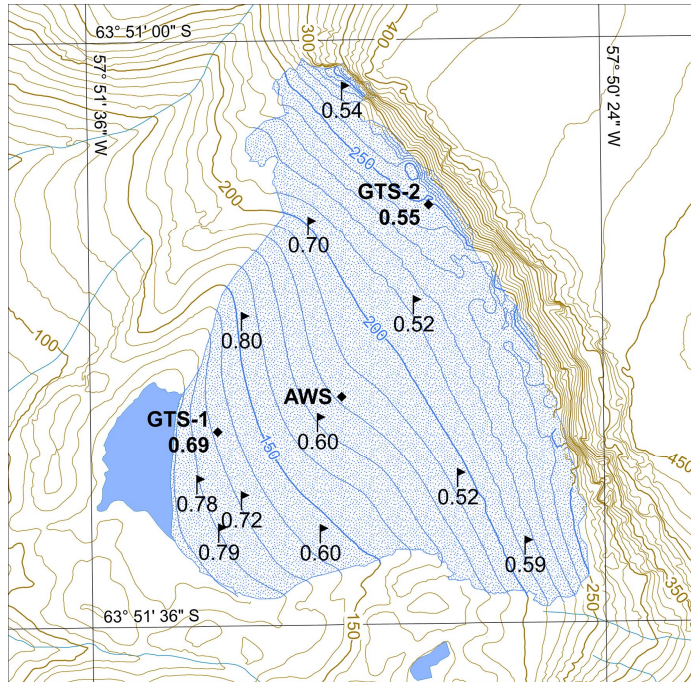


Fig. 3. Surface lowering of Triangular Glacier measured at ablation stakes from 20 January to 23 February 2022.

Site	Longitude (°W)	Latitude (°S)	Altitude (m a.s.l.)	Aspect (°)	Slope (°)	Topographic shielding factor	Duration of direct incoming solar radiation over DJF (h)	Ablation at un/covered surface from 6 Jan. to 23 Feb. 2022 (m)
AWS	-57.850193	-63.856101	180	223	8.8	0.974	866.1	0.77/-
GTS-1	-57.855047	-63.856677	114	253	13.3	0.982	941.6	0.78/0.37
GTS-2	-57.846718	-63.852825	273	225	7.7	0.864	605.9	0.60/0.36

Table 1. Automatic weather station (AWS) and geotextile test sites (GTS) characteristics.

Results

The summer 2021/22 (herein defined as the period from 1 December 2021 to 23 February 2022) was a remarkably warm period in the north-western part of James Ross

Island, with the mean summer air temperature on Triangular Glacier AWS of 1.7°C, the lowest daily mean air temperature of -2.1°C on 15 January 2022 and the high-

est daily mean of 8.6°C on 7 February 2022 (Fig. 4a). Positive air temperatures prevailed during periods 1–27 December, 18–26 January, and 4–12 February, with the highest temperature of 13.4°C recorded on 7 February 2022. Fig. 4a shows daily changes in theoretical sunshine duration from 20.9 hours during the summer solstice to 15.0 hours at the end of the experimental period, which confirms that warm periods are controlled by the horizontal advection of air masses rather than the solar irradiance variation. The three prominent cooling periods with temperatures below -1.5°C observed between 30 December and 1 January, from 13 to 15 January, and from 16 to 18 February were related with snowfall events. The PDD sum was 183.6 K d⁻¹ over the summer with the highest PDD of 67.9 K d⁻¹ in December and the lowest (56.7 K d⁻¹) in February (Table 2).

The ultrasonic measurement at the AWS

show glacier surface lowering of 146.5 cm from 1 December to 23 February, with the mean summer rate of 1.7 cm d⁻¹ (Fig. 4b). While the cumulative sum of the negative change of surface elevation due to snow melt, wind drift, and sublimation exceeded 249 cm, the cumulative sum of the positive change involving short-term snowfall and accumulation was 102.4 cm (Table 2). The longest period with surface lowering of 96.7 cm was observed between 1 and 28 December, with a mean rate of 3.5 cm d⁻¹. Over the same period, the mean daily air temperature was 2.2°C and PDD sum reached 66.7 K d⁻¹. The highest melt rate of 10 cm d⁻¹ was recorded in the mid-summer (22/23 and 30/31 January) during the period of the warm air advection accompanied by temperatures above 6.5°C. The maximum surface increase of up to 18 cm was registered on 2-3 and 10-11 January due to heavy snowfall during the cold air advection from the northeast to the east.

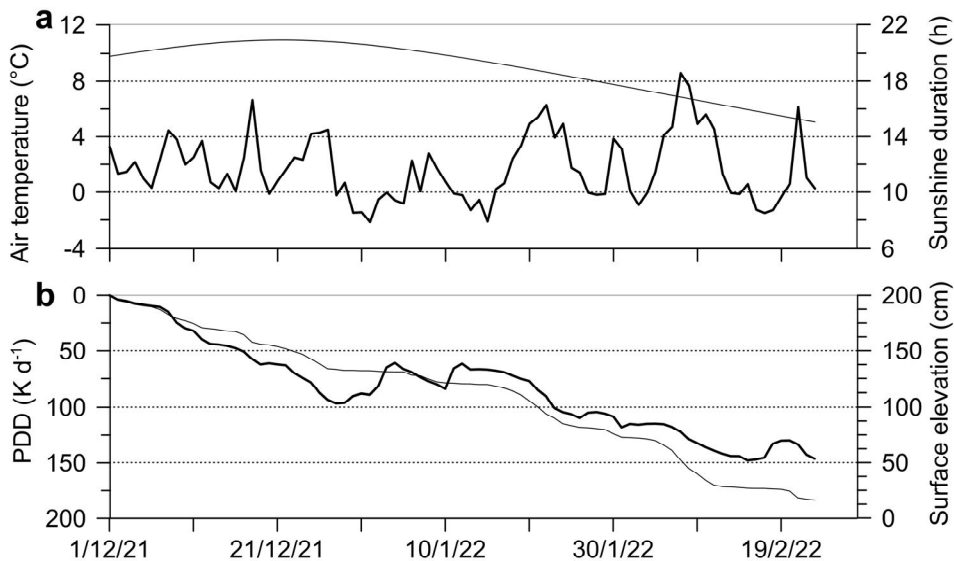


Fig. 4. (a) Changes of air temperature (thick line), theoretical sunshine duration (thin line), (b) positive degree-day (PDD) sum (thin line), and glacier surface elevation (thick line) during the summer 2021/22 at Triangular Glacier.

The surface lowering of 69.2 cm (1.4 cm d^{-1}) was recorded at the AWS over the duration of the cover experiment from 6 January to 23 February. Triangular Glacier was completely snow-covered at the beginning of this period and a snowstorm on 11 January increased its surface with 16 to 24 cm of fresh snow (Fig. 5). More than 5 cm of the snow was drifted away by wind over the next 24 hours, but cold conditions and high albedo of the snowpack reduced the surface melt during subsequent days. An increase in temperature and direct sunshine after 15 January prompted the snow melt disrupting the continuous

snow pack on 21 January. The areas of bare ice surface progressively increased and the remaining snow disappeared from the glacier terminus before the end of January. A snowfall and freezing conditions at the beginning of February reduced the surface melt that started to increase again with rising temperatures after 5 February. The enhanced melt culminated between 7 and 9 February with the mean lowering rate of $6\text{--}7 \text{ cm d}^{-1}$. Occasional snowfall and low temperatures after 12 February decelerated the surface melt that decreased glacier surface at a mean rate of 1.2 cm d^{-1} until the end of the experimental period (Fig. 5).

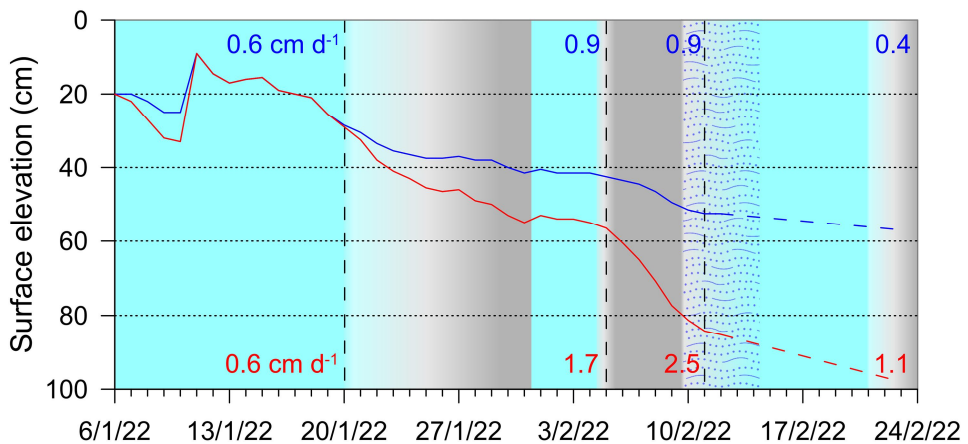


Fig. 5. Surface elevation change at the glacier surface (red line) and geotextile-covered site (blue line) between January 6 and February 23 2022. Dashed lines connect the daily records with final surface elevation on February 23. Blue and red values in the plot indicate relevant mean ablation rate for the sub-periods indicated by vertical dashed lines.

The lowering rate at the experimental sites covered with the geotextile was lower compared to the unprotected glacier surface during the major part of the experimental period. At the beginning of this period, the protected snow surface decreased by less than 3 cm d^{-1} while the uncovered surface experienced the lowering rate of up to 5 cm d^{-1} . From 11 to 20 January the lowering rate of the un/protected surfaces was equal as the geotextile protection was covered with snow. The difference in the

lowering rates at the un/protected sites started to increase with the rising amount of water in the snowpack. The maximum difference was observed from 6 to 9 February (Fig. 6), when high air temperature prompted surface melt on the glacier whereas the geotextile cover reduced the heat flux to the protected snow and ice. During this period, the lowering rate at the protected surface ranged from 1 to 3 cm d^{-1} whereas the unprotected surfaces decreased by 4 to 6 cm d^{-1} .

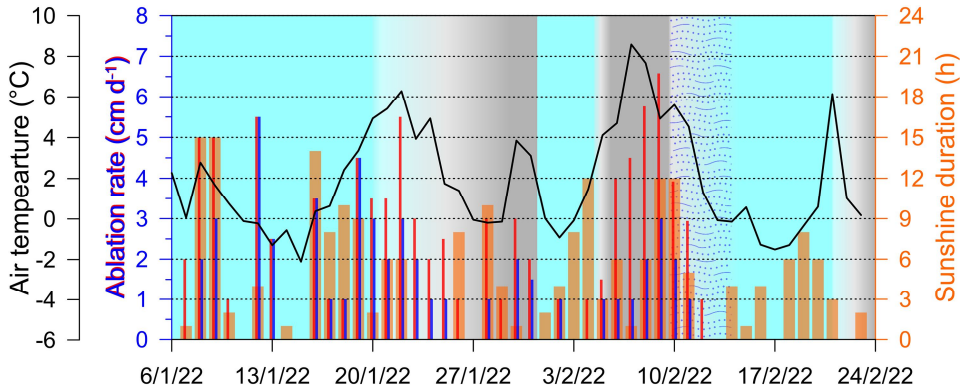


Fig. 6. Ablation rate at the glacier surface (red bars) and geotextile-covered site (blue bars). Orange bars show the direct sunshine duration and black line marks daily air temperature recorded at the test site. Cyan and grey rectangles indicate periods with continuous snow cover and bare glacier surface, respectively, blue hatches represent superimposed ice.

Month	AT (°C)	PDD (°K d ⁻¹)	ΣNEG	ΣPOS
December	1.9	67.9	97.8	9.5
January	1.3	59.0	86.5	56.5
February	2.0	56.7	64.7	36.3
Mean/Sum	1.7	183.6	249.0	102.4

Table 2. Mean air temperature (AT), positive degree-day (PDD) sum, and sum of negative (ΣNEG) / positive (ΣPOS) surface elevation changes at Triangular Glacier during the summer 2021/22.

The lowering of the unprotected glacier surface recorded at the experimental sites is within the range of values observed at the ablation stakes, and the data from the GTS-1 and GTS-2 sites represent well the glacier area of high and low ablation, respectively (Fig. 3).

The surface lowering was more prominent at the GTS-1 site, where the glacier surface decreased by 78 cm over the experimental period at a mean rate of 1.66 cm d⁻¹. By contrast, the surface elevation at the glacier head (GTS-2) decreased by 60 cm yielding a mean lowering rate of 1.28 cm d⁻¹. The elevation change of the glacier surface protected by the geotextile is nearly the same at both GTS-1 and GTS-2 sites as demonstrate the lowering rates of 0.79 and 0.77 cm d⁻¹, respectively. The larger difference in the lowering rates determined for the natural and protected

glacier surface at the GTS-1 site (Fig. 7) indicates a more pronounced effect of the geotextile protection at the glacier terminus compared to the glacier head. At the GTS-1 site, 33 cm of snow melted at both un/protected surfaces but only 4 cm of ice ablated under the geotextile cover compared to 45 cm of melted ice at the unmanaged surface. As a result, total ablation equals 0.53 m w.e. at the unprotected surface and 0.16 m w.e. under the geotextile cover. These values indicate that the surface ablation was reduced to a 69% reduction of natural ablation. The ablation at the GTS-2 site consists of snow melt only with a total surface lowering of 60 cm at the unprotected glacier and 36 cm under the geotextile cover. The corresponding ablation of 0.23 and 0.14 m w.e. reveals that the geotextile reduced the melt rate by 40% at this site.

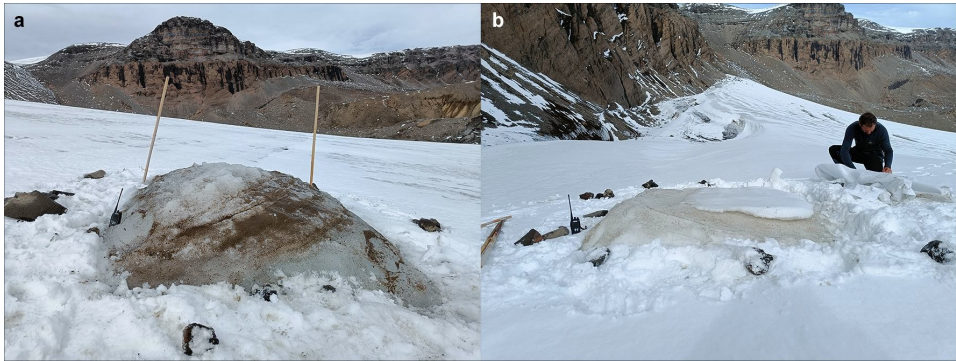


Fig. 7. Effect of the geotextile protection at the GTS-1 (a) and GTS-2 (b) sites at the end of the experiment period (6 January to 23 February 2022).

Discussion

Considering the small differences in the surface elevation, aspect and slope across the Triangular Glacier, the main reason for different microclimate conditions and melt rates at the geotextile experimental sites may be attributed to topographic shielding (Table 1). The GTS-2 site is shaded by a vertical headwall until noon throughout the summer, experiencing 64% of the direct incoming solar radiation compared to the GTS-1 site. As a result, the glacier terminus receives more downward solar radiation and melts more rapidly than the shaded site at the glacier head. The melt rate at these two sites differs remarkably at the unprotected glacier surface and only slightly under the geotextile cover. The higher variability of the melt rate determined for the natural glacier surface drives the efficiency of the geotextile that reflects the ability to reduce the melting with respect to the melt rates at the unprotected areas (Huss et al. 2021). The calculated 69% and 40% reduction of the natural surface melt supports higher efficiency of the geotextile protection at sites with maximum solar radiation input as suggested by Huss et al. (2021).

The effect of the geotextile decreases when continuous snowpack forms and per-

sists on the glacier surface for a substantial period of the melt season. The snowpack that formed at Triangular Glacier during the snowfall on 11 January reduced the period of glacier exposure to solar radiation by 10 days, which represent 20% of the experimental period. During this time, snow cover protected the glacier surface from temperature effects and eliminated direct insolation, significantly reducing melting on the bare glacier surface and under the geotextile. By contrast, the difference in the melt rates at the unmanaged and the protected surfaces increased during warm clear-sky days when the snow melted. The largest difference in the melt rates at the un/protected surfaces coincides with the period of the bare glacier surface (covered with a thin dust cover) after 6 February implying the primary importance of surface reflectivity (e.g. Olefs and Lehning 2010).

The effect of the geotextile cover on the surface melt observed on Triangular Glacier is consistent with most of the reported estimates (Table 3). The efficiency of 40–69% determined at this glacier overlaps with the efficiency range of 50–70% derived for glaciers in the European Alps (Huss et al. 2021) but exceeds the values determined in the high-mountain regions of

Region	Site	Latitude	Altitude (m a.s.l.)	Clear-sky downward solar radiation at noon (W m^{-2})	Summer sun elevation ($^{\circ}$)	Experiment duration (d)	Uncovered surface ablation (m)	Melt reduction (%)	Reference
Qionglai Shan	Dagu Glacier	32°13'30"N	4830	1036.1–967.4	81.2–66.4	63	1.1	34	Xie et al. (2022)
Lesser Caucasus	Mount Aragats	40°28'40"N	3200	1000.6–892.3	73.0–58.2	37, 35	-	42–57	Nestler et al. (2014)
Tien Shan	Urumqi Glacier No. 1	43°07'30"N	3800	984.3–863.5	70.3–55.5	65	2.5	29	Liu et al. (2022)
Alps	Presena Ovest Glacier	46°13'23"N	2765	962.3–827.4	67.2–52.4	77, 85	-	49–73	Sensse et al. (2020)
	Dosdè Est Glacier	46°23'26"N	2800	961.1–825.4	67.0–52.2	112	3.7	69	Sensse et al. (2020)
	Schaufelferner	46°59'N	2870	956.5–818.1	66.5–51.7	85/121	2.7/3.8	60	Olefs and Fischer (2008)
James Ross Island	Triangular Glacier	63°51'24"S	114	837.3–586.8	49.6–34.1	47	0.7	40–69	This study

Table 3. Melt season characteristics and ablation at mid- to high-latitude experiment sites.

Central Asia (Liu et al. 2022, Xie et al. 2022). In these regions, summer ablation on glaciers coincides with the maximum accumulation that occurs from May to September, and represents up to 88% of annual precipitation (Sun et al. 2015). Frequent snowfall increases the reflectivity of snow-covered glacier surface, reducing the effect of the geotextile protection on the surface melt. Moreover, the artificial cover precludes accumulation of snow on the surface of a glacier and its plausible transformation in glacier ice.

Summer snowfalls also suppress the melting of Triangular glacier, as indicated by 6 snowfall events recorded during the summer 2021/22. Nevertheless, it is worth mentioning that the experimental period belongs to the warmest summers on Triangular Glacier since the beginning of the mass-balance measurements in 2014/15 (Engel et al. 2022). The mean air temperature calculated for the summer 2021/22 is about 0.8 to 1.2°C warmer than the 2020/21 and 2019/2020 summer periods. The singularity of the summer period 2021/22 coincides well with the recent climate change over the Antarctic Peninsula and a reported increase in heatwave magnitude by 0.4°C with respect to the 1950–1984 period (González-Herrero et al. 2022). An example of such an event is the anomalously warm February 2020, when an unprecedented heatwave period was observed in the continental Antarctic region, with the highest air temperature of 18.3°C recorded on 6 February at the Esperanza station (Francelino et al. 2021).

The surface lowering recorded over the summer 2021/22 on Triangular Glacier is lower compared to the lowering rates in mid-latitude regions. The total surface lowering of 1.5 m recorded at the AWS during the summer months and the surface elevation changes observed at the ablation stakes over a four-week period imply a total melt-season ablation of 1.3 to 1.6 m, which is at least two times lower than in the Alps (Olefs and Fischer 2008, Sommer

et al. 2020). The lower ablation in the study area reflects colder conditions, less intense incoming solar radiation, and a shorter melt season in the northern part of James Ross Island. The mean air temperature of 1.7°C recorded during the 2021/22 summer period at Triangular Glacier is well below the mean summer (JJA) temperature of 3.1 to 7.1°C that represent elevation range of 2500–3100 m a.s.l. in the Alps (the GISTEMP v4 data for Kredarica,

Zugspitz, and Sonnblick stations in the period 2001–2021^[21]; Lenssen et al. 2019). The clear-sky downward solar radiation at noon in the northern part of James Ross Island is 125 to 240 W m⁻² lower (Table 3) and the melt season is up to two months shorter compared to the Alps (4 to 5 months according to Thibert et al. 2013) but the relative impact of these factors on the surface melt at Triangular Glacier remains unclear.

Conclusions

Triangular Glacier experienced increased air temperatures and enhanced surface melt during the summer 2021/22, which was the warmest melt season since the beginning of the local climate measurements in 2014. The mean air temperature of 1.7°C and the positive degree-day sum of 183.6°K d⁻¹ was calculated for the period from 1 December 2021 to 23 February 2022. As a result of these unprecedented warm conditions, the glacier surface decreased by around 1.5 m over the summer. From 6 January to 23 February, the surface lowering ranged from 0.8 m on the glacier terminus to 0.5 m at the top of

the glacier shaded by headwall cliffs.

The geotextile cover installed at the glacier terminus and the head sites reduced the surface melt by 69% and 40%, respectively. Variable reduction of the glacier melt indicates higher efficiency of the geotextile protection for sites unconstrained by topography where solar radiation input is not limited. The efficiency of the geotextile cover determined at Triangular Glacier falls within the range of the values reported from the mid-latitude glaciers where the geotextile cover reduces the snow and ice melt by 30 to 70%.

References

- BIRD, R. E., HULSTROM, R. L. (1981): *A simplified clear sky model for direct and diffuse insolation on horizontal surfaces*. Solar Energy Research Institute, Golden, CO. 38 p. doi: 10.2172/6510849
- BLISS, A. K., CUFFEY, K. M. and KAVANAUGH, J. L. (2011): Sublimation and surface energy budget of Taylor Glacier, Antarctica. *Journal of Glaciology*, 57(204): 684-696. doi: 10.3189/002214311797409767
- BURKHART, P. A., ALLEY, R. B., THOMPSON, L. G., BALOG, J. D., BALDAUF, P. E. and BAKER, G. S. (2017): Savor the cryosphere. *GSA Today*, 27: 4-10. doi: 10.1130/GSATG293A.1
- CUFFEY, K. M., PATERSON, W. S. B. (2010): *The physics of glaciers*. Butterworth-Heinemann, Amsterdam. 704 p.
- EDWARDS, T. L. and 83 others (2021): Projected land ice contributions to twenty-first-century sea level rise. *Nature*, 593: 74-82. doi: 10.1038/s41586-021-03302-y
- ENGEL, Z., LÁSKA, K., KAVAN, J. and SMOLÍKOVÁ, J. (2022, *in press*): Persistent mass loss of Triangular Glacier, James Ross Island, north-eastern Antarctic Peninsula. *Journal of Glaciology*. doi: 10.1017/jog.2022.42

- FRANCELINO, M. R., SCHAEFER, C., SKANSI, M. D. L. M., COLWELL, S., BROMWICH, D. H., JONES, P., KING, J. C., LAZZARA, M. A., RENWICK, J., SOLOMON, S., BRUNET, M. and CERVENY, R. S. (2021): WMO evaluation of two extreme high temperatures occurring in February 2020 for the Antarctic Peninsula region. *Bulletin of the American Meteorological Society*, 102(11): E2053-E2061. doi: 10.1175/BAMS-D-21-0040.1
- GONZÁLEZ-HERRERO, S., BARRIOPEDRO, D., TRIGO, R.M., LÓPEZ-BUSTINS, J. A. and OLIVA, M. (2022): Climate warming amplified the 2020 record-breaking heatwave in the Antarctic Peninsula. *Communications Earth & Environment*, 3: 122. doi: 10.1038/s43247-022-00450-5
- HOCK, R. (2003): Temperature index melt modelling in mountain areas. *Journal of Hydrology*, 282(1–4): 104–115. doi: 10.1016/S0022-1694(03)00257-9
- HOCK, R., HUTCHINGS, J. K. and LEHNING, M. (2017): Grand challenges in cryospheric sciences: Toward better predictability of glaciers, snow and sea ice. *Frontiers in Earth Science*, 5: 64. doi: 10.3389/feart.2017.00064
- HUGONNET, R., MCNABB, R., BERTHIER, E., MENOUNOS, B., NUTH, C., GIROD, L., FARINOTTI, D., HUSS, M., DUSSAILLANT, I., BRUN, F. and KÄÄB, A. (2021): Accelerated global glacier mass loss in the early twenty-first century. *Nature*, 592: 726–731. doi: 10.1038/s41586-021-03436-z
- HUSS, M., SCHWYN, U., BAUDER, A. and FARINOTTI, D. (2021): Quantifying the overall effect of artificial glacier melt reduction in Switzerland, 2005–2019. *Cold Regions Science and Technology*, 184: 103237. doi: 10.1016/j.coldregions.2021.103237
- LAFFIN, M. K., ZENDER, C. S., VAN WESSEM, M. and MARINSEK, S. (2022): The role of föhn winds in eastern Antarctic Peninsula rapid ice shelf collapse. *The Cryosphere*, 16: 1369–1381. doi: 10.5194/tc-16-1369-2022
- LENSSEN, N., SCHMIDT, G., HANSEN, J., MENNE, M., PERSIN, A., RUEDY, R. and ZYSS, D. (2019): Improvements in the GISTEMP uncertainty model. *Journal of Geophysical Research: Atmospheres*, 124(12): 6307–6326. doi: 10.1029/2018JD029522
- LI, Y. (2013): Determining topographic shielding from digital elevation models for cosmogenic nuclide analysis: A GIS approach and field validation. *Journal of Mountain Science*, 10: 355–362. doi: 10.1007/s11629-013-2564-1
- LIU, S., WANG, F., XIE, Y., XU, C., XUE, Y., YUE, X. and WANG, L. (2022): Quantifying the artificial reduction of glacial ice melt in a mountain glacier (Urumqi Glacier No. 1, Tien Shan, China). *Remote Sensing*, 14: 2802. doi: 10.3390/rs14122802
- NAVARRO, F. J., JONSELL, U. Y., CORCUERA, M. I. and MARTÍN-ESPAÑOL, A. (2013): Decelerated mass loss of Hurd and Johnsons Glaciers, Livingston Island, Antarctic Peninsula. *Journal of Glaciology*, 59(213): 115–128. doi: 10.3189/2013JG12J144
- NESTLER, A., HUSS, M., AMBARTZUMIAN, R. and HAMBARIAN, A. (2014): Hydrological implications of covering wind-blown snow accumulations with geotextiles on Mount Aragats, Armenia. *Geosciences*, 4: 73–92. doi: 10.3390/geosciences4030073
- OERLEMANS, J., HAAG, M. and KELLER, F. (2017): Slowing down the retreat of the Morteratsch glacier, Switzerland, by artificially produced summer snow: A feasibility study. *Climatic Change*, 145: 189–203. doi: 10.1007/s10584-017-2102-1
- OLEFS, M., OBLEITNER, F. (2007): Numerical simulations on artificial reduction of snow and ice ablation. *Water Resources Research*, 43: W06405. doi: 10.1029/2006WR005065
- OLEFS, M., FISCHER, A. (2008): Comparative study of technical measures to reduce snow and ice ablation in Alpine glacier ski resorts. *Cold Regions Science and Technology*, 52: 371–384. doi: 10.1016/j.coldregions.2007.04.021
- OLEFS, M., LEHNING, M. (2010): Textile protection of snow and ice: measured and simulated effects on the energy and mass balance. *Cold Regions Science and Technology*, 62: 126–141. doi: 10.1016/j.coldregions.2010.03.011
- ORLOVE, B., WIEGANDT, E. and LUCKMAN, B. N. (2008): The place of glaciers in natural and cultural landscapes. In: B. Orlove, E. Wiegandt and B. N. Luckman (eds.): *Darkening Peaks*. University of California Press, Berkeley, pp. 3–19.
- PEIXOTO, J. P., OORT, A. H. (1992): *Physics of Climate*. Springer-Verlag, New York, Berlin, Heidelberg, 520 p.

- SAUTER, T., GALOS, S. P. (2016): Effects of local advection on the spatial sensible heat flux variation on a mountain glacier. *The Cryosphere*, 10: 2887-2905. doi: 10.5194/tc-10-2887-2016
- SENESE, A., AZZONI, R. S., MARAGNO, D., D'AGATA, C., FUGAZZA, D., MOSCONI, B., TRENTI, A., MERALDI, E., SMIRAGLIA, C. and DIOLAIUTI, G. (2020): The non-woven geotextiles as strategies for mitigating the impacts of climate change on glaciers. *Cold Regions Science and Technology*, 173: 103007. doi: 10.1016/j.coldregions.2020.103007
- SKOGSBERG, K., LUNDBERG, A. (2005): Wood chips as thermal insulation of snow. *Cold Regions Science and Technology*, 43: 207-218. doi: 10.1016/j.coldregions.2005.06.001
- SOMMER, C., MALZ, P., SEEHAUS, T. C., LIPPL, S., ZEMP, M. and BRAUN, M. H. (2020): Rapid glacier retreat and downwasting throughout the European Alps in the early 21st century. *Nature Communications*, 11: 3209. doi: 10.1038/s41467-020-16818-0
- SUN, M., LI, Z., YAO, X., ZHANG, M. and JIN, S. (2015): Modeling the hydrological response to climate change in a glacierized high mountain region, northwest China. *Journal of Glaciology*, 61(225): 127-136. doi: 10.3189/2015JoG14J033
- THOST, D. E., TRUFFER, M. (2008): Glacier recession on Heard Island, Southern Indian Ocean. *Arctic, Antarctic, and Alpine Research*, 40(1): 199-214. doi: 10.1657/1523-0430(06-084) [THOST]2.0.CO;2
- THIBERT, E., ECKERT, N. and VINCENT, C. (2013): Climatic drivers of seasonal glacier mass balances: an analysis of 6 decades at Glacier de Sarennes (French Alps). *The Cryosphere*, 7: 47-66. doi: 10.5194/tc-7-47-2013
- XIE, Y., WANG, F., XU, C., YUE, X., YANG, S. and HUANG, S. (2022, *under review*): Applying artificial cover to reduce the melting of the Dagu Glacier, the East Qinghai-Tibetan Plateau. *Advances in Climate Change Research*. doi: 10.2139/ssrn.4215361

Web sources / Other sources

- [1] Czech Geological Survey (2009): *James Ross Island – northern part. Topographic Map 1 : 25,000*. Czech Geological Survey, Praha.
- [2] GISTEMP Team (2022): *GISS Surface Temperature Analysis (GISTEMP), version 4*. NASA Goddard Institute for Space Studies. Dataset accessed 2022-12-12 at <https://data.giss.nasa.gov/gistemp/>